Ultra-Wideband Time-of-Arrival and Angle-of-Arrival Estimation Using Transformation Between Frequency and Time Domain Signals

Naohiko Iwakiri and Takehiko Kobayashi
Tokyo Denki University, Chiyoda-ku, Tokyo 101-8457, Japan
Email: iwakiri@grace.c.dendai.ac.jp, koba@c.dendai.ac.jp

Abstract—**This paper presents an ultra wideband (UWB) channel sounding scheme with a technique for time of arrival (TOA) and angle of arrival (AOA) estimation using transformation between time and frequency domain signals. Since the measured UWB power spectrum can be transformed into a time domain signal, both frequency and time domain signals are available for the channel estimation. We propose the TOA estimation using a peak search over time domain signal, and the AOA estimation using MUSIC and AOA histograms. The AOA histogram is counted for AOA samples of discrete frequencies over the UWB bandwidth. Comparing both AOA histograms before and after TOA subtraction, we can determine pairing the elements of TOA vector and those of AOA vector. The anechoic chamber tests indicated that both TOAs and AOAs were precisely resolved for two-path model, even if either TOAs or AOAs were too close to resolve.**

Index Terms— **Angle of arrival, antenna arrays, Cramér–Rao Bound (CRB), multiple signal classification (MUSIC), radio channel measurement and estimation, time of arrival, ultrawide- band (UWB) propagation**

I. INTRODUCTION

Wideband digital wireless communications are becoming increasingly practical in indoor environments. Therefore, it is important to clarify channel environments using an effective measurement and precise channel parameter estimation. In microwave or ultra wideband (UWB) channel environments, one widely used technique is measuring the channels with multiple antennas at the transmitter and/or receiver and estimating several channel parameters based on the measurement data and specific channel models [1]–[16]. In UWB indoor environments, assuming a static channel, a vector network analyzer (VNA) and single-element antenna with a spatial scanner have been widely used to measure the environments [5]. The former uses the transmitter and receiver, the latter is formed from a three-dimensional virtual antenna array. There has been much work on estimating channel parameters for the UWB, such as space-alternating generalized expectation-maximization algorithm (SAGE) [5], CLEAN [6]. It was shown in [5] that the resolution of the time of arrival (TOA) was more than 0.67 ns and that of the angle of arrival (AOA) was more than 10°. Many of the estimation methods are based on maximum likelihood (ML) estimation or a family of subspace algorithms such as multiple signal classification (MUSIC). To obtain the precise signal model for measurement data in practice, the signal models must be formed taking the characteristics of the measuring instruments into consideration even if the model is theoretically perfect. We proposed a technique for joint TOA and AOA estimation of UWB signals using time domain (TD) smoothing [14]. The TOA and AOA could be estimated using simple method, the former adopted a peak search in TD signals and the latter adopted an one-dimensional (1-D) MUSIC in frequency domain (FD) signals. The transformation between TD and FD signals used a Fourier transform. We showed that the resolution of TOA was more than 1 ns, that of AOA was more than 3° for an element spacing of half wavelength at more than 3 dB for the case of two paths. However, we did not discuss about the specific TOA and AOA estimation algorithm over the UWB and the resolution of closely spaced TOAs as well as AOAs.

In this paper, we improve the previous algorithm, and then propose the TOA estimation using a peak search over TD signals and the AOA estimation using AOA histograms for the two-path model. Since the AOA histogram is counted for AOA samples of all discrete frequencies over the UWB, each AOA sample can be estimated using MUSIC algorithm with a uniform linear array (ULA). Therefore, the AOA estimation of the UWB signals exploits MUSIC algorithm of narrowband assumption and the measurement data observed by the simple antenna array with fixed element spacing. The AOA histogram is also available for pairing the elements of TOA vector and those of AOA vector. If both TOAs and AOAs are resolved, pairing the elements can be determined using the AOA histograms before and after the TOA subtraction. Moreover, even if either TOAs or AOAs are too close to resolve, we can determine pairing the elements using the same method.

This paper is organized as follows: The UWB signal models consisting of the VNA with the spatial scanner are described in Section II. The TOA and AOA estimation algorithm and the RMSE simulations to evaluate the resolution of estimated TOA and AOA are

discussed in Section III. The test results for two-path model in the anechoic chamber are presented in Section IV. Finally, the conclusions are drawn in Section V.

II. UWB SIGNAL MODELS

The array signal model was derived from the narrowband assumption [1], [17]. It is assumed that a finite number L of plane waves impinges on a receiver using an antenna array and channel parameters of the waves are constant over the whole bandwidth. For M-element antenna array of arbitrary geometry, the array output vector is given by:

$$\mathbf{y}(t) = \sum_{l=1}^{L} \mathbf{s}(t;\boldsymbol{\theta}_l) + \mathbf{n}(t), \tag{1}$$

where $\mathbf{y}(t) = [y_1, \cdots, y_M]^T$ is the received signal vector, $\mathbf{s}(t;\boldsymbol{\theta}_l)$ is the contribution of the l th wave to the M baseband signals at the array, $\mathbf{n}(t) = [n_1, \cdots, n_M]^T$ is an $M \times 1$ vector of white Gaussian noise. We assume that the channel parameters of the l th wave is denoted by $\boldsymbol{\theta}_l = [\phi_l, \tau_l]$, where ϕ_l is the azimuth AOA and τ_l is the TOA. The physical observation model is given by:

$$\mathbf{z}(t) = \sum_{l=1}^{L} \mathbf{v}(\phi_l)\, a_l u(t - \tau_l) + \mathbf{n}(t), \tag{2}$$

where $\mathbf{v}(\phi_l) = [v_1(\phi_l), \cdots, v_M(\phi_l)]^T$ is the steering vector, a_l is complex amplitude, $u(t-\tau_l)$ is the signal shape and $\mathbf{z}(t) = [z_1, \cdots, z_M]^T$.

The VNA transmits and receives a sine wave signal. If we use P sine waves and each wave is swept over the UWB band, this signal can be treated as the FD UWB signals. Let $Y_m(k)$ denote the received k th sine wave signal at the m th array element. The FD signals are given by taking the N points discrete Fourier transform (DFT)

$$Y_m(k) = \sum_{n=0}^{N-1} y_m(n) e^{-j(2\pi/N)kn}, \quad k = 0,1,\cdots,N-1, \tag{3}$$

where N is a power of 2. If P is $2^{b-1} < P < 2^b = N$, where b is an integer, P points FD UWB signals are added $N - P$ padding bits to obtain N points DFT.

We can obtain the TD UWB signals corresponding to the FD UWB signals taking inverse DFT (IDFT) with respect to $Y_m(k)$ as

$$y_m(n) = \frac{1}{N} \sum_{k=0}^{N-1} Y_m(k) e^{j(2\pi/N)kn}, \quad n = 0,1,\cdots,N-1. \tag{4}$$

We assume that the time t of equation (1) and (2) is equal to discrete time n of equation (3) and (4). In this paper, we use the fast Fourier transform (FFT) and the inverse FFT (IFFT) to calculate the DFT and the IDFT, respectively.

If $z_m(t)$ is equivalent to $y_m(n)$, the channel parameters can be estimated precisely. However, since $z_m(t)$ is the signal based on the narrowband assumption and $y_m(t)$ is the TD UWB signals taking IFFT with respect to the measured VNA signals, $z_m(t)$ and $y_m(t)$ are not exactly equivalent. Then we should develop the UWB channel estimation scheme taking this problem into consideration.

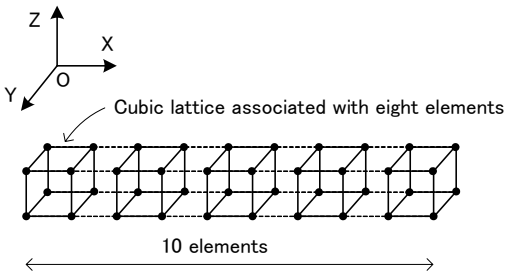

Figure 1. Array geometry with cubic lattices and $10 \times 2 \times 2$ ULA.

III. TOA AND AOA ESTIMATION SCHEME

A. Smoothing Techniques of Measured VNA Signal

The UWB signal measured by VNA has four basic properties as follows: (1) there is only one snapshot; (2) the reflected and/or scattered signals correlate strongly; (3) the power spectrum is not flat over the UWB bandwidth because of nonlinear parts and antennas; (4) there are FD discrete signals, since each of the VNA transmitted signal is a sine wave. We need to consider those properties to improve the quality of measurements.

If the IF bandwidth of the VNA is set low, such as 100 Hz, the data of each frequency sample at one element is averaged, respectively. Then FD smoothing can be performed. For the AOA estimation, the MUSIC with forward-backward (FB) spatial smoothing can be used to remove the singularity between signals impinging on the antenna array. Then spatial domain smoothing can be performed. To improve one snapshot limitation, we adopted another domain smoothing which is referred to as TD smoothing [14] using the three dimensional antenna array associated with $10 \times 2 \times 2$ elements which consist of four $10 \times 1 \times 1$ ULAs, as shown in Fig. 1. The solid lines form a cubic lattice associated with eight elements and the number of available cubic lattices are five. TD smoothing is averaged over these eight elements of each cubic lattice.

B. TOA and AOA Estimation Algorithm

We assume that two waves impinge on the antenna array and two unknown channel parameter vectors, the AOA vector $\boldsymbol{\phi} = [\phi_1, \phi_2]^T$ and the TOA vector $\boldsymbol{\tau} = [\tau_1, \tau_2]^T$. The experimental setup of test system is shown in Fig. 2. The specification for radio anechoic chamber tests is listed in Table I. After measuring signals for all elements of the virtual antenna array, we perform the TOA and AOA estimation algorithm using transformation between FD and TD signals as follows.

1) A cubic lattice is selected and added 273 padding bits to 751 FD samples corresponding to measured power spectrum of each eight element set.
2) The total of 1024 samples for each element set is taken the IFFT to obtain the TD signal.

3) TD smoothing is performed across each element set.
4) After 1)–3) are repeated for the cubic lattices over the antenna array, one or two strongest peaks are selected from the TD signals of each element associated with the ULA, then TOAs corresponding to the peaks at each element are determined.
5) The total 751 of AOA samples over measured power spectrum are estimated using the 1-D MUSIC algorithm with 1-D FB spatial smoothing.
6) The AOA histogram of 5) before TOA subtraction is calculated and one or two strongest peaks are selected, then the AOAs before TOA subtraction are estimated.
7) If two TOAs and/or AOAs exist, several TD samples around single TOA in ascending order of the relative delay are subtracted from the TD signals of each element associated with the ULA.
8) Taking FFT with respect to the TD signals, the total 751 of AOA samples after the TOA subtraction at each frequency point are estimated using the same manner as 5).
9) The AOA histograms of 8) after TOA subtraction are calculated, and then the AOAs after TOA subtraction are estimated.
10) If more than single TOA and/or AOA exist, pairing the elements of TOA vector and those of AOA vector is determined using AOA histograms before and after TOA subtraction.

C. RMSE Performances of AOA Estimation

The AOA estimation is characterized by the root mean-square estimation error (RMSE). If it is possible to minimize the RMSE when the bias is zero, the variance can also be minimized. If the channel parameters are resolved using the covariance matrix for a static channel, the estimation accuracy improves as the SNR increases and/or the number of snapshots increases. The variance of estimated parameters then approaches the Cramér–Rao Bound (CRB) [1], [8], [17] and [18]. When several AOAs are estimated individually, the CRB of the ULA can be obtained in [17] as:

$$C_{CRB} = \frac{1}{K}\left[\frac{1}{ASNR} + \frac{1}{ASNR^2}\right]\frac{6}{M^2 - 1}, \qquad (5)$$

where K is the number of snapshots, M is the number of antenna array elements and $ASNR = M \times SNR$. When there are two paths, the criterion of path separation is given by the standard beamwidth $2\pi / M$ [17], [19]. The beamwidth for the 10-element ULA is 0.63, which implies that two paths need to be at least 12° apart.

We simulated the RMSE performance of the AOA estimation before and after TOA subtraction for two-path model with equal signal powers. The simulation specifications were set the same parameters as radio anechoic chamber tests in Table I. The AOA was estimated using the 1-D MUSIC algorithm with 1-D FB spatial smoothing for the 10-element ULA. We adopted an ideal UWB spectrum model which power was flat over the UWB for one-path model. The signal power was set -56.0 dB, which value was a mean power of the test system. White Gaussian noise was added each frequency point according to setting SNR. The simulated FD and TD signals at SNR = 20 dB are shown in Fig. 3 (a) and (b), respectively. The TOAs and the AOAs set the same parameters as scenario A in Table II. We assumed the number of paths was known, and thus the number of paths before and after TOA subtraction was two and one, respectively. The MUSIC spectra corresponding to three frequencies, 3.1, 5.0 and 10.0 GHz before TOA subtraction at SNR = 20 dB are plotted in Fig. 4. We can see two peaks corresponding to two paths for scenario A. The spectrum is sharper as the frequency increases, since the element spacing is 15 mm which corresponds to half a wavelength at 10.0 GHz and 0.15 wavelengths at 3.1 GHz.

We first discuss the RMSE performances of the AOA estimation before and after TOA subtraction for four frequencies, 3.1, 5.0, 8.0 and 10.0 GHz, as shown in Figs. 5 and 6. The RMSE performances for 200 trials and its CRB (K=1, M=9) at SNR going from -20 dB to 20 dB is

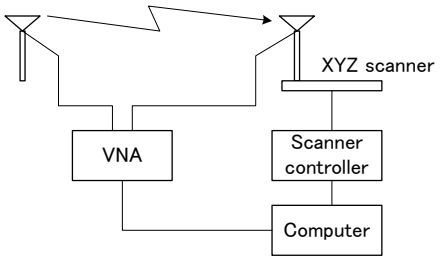

Figure 2. The experimental setup of test system.

TABLE I.
SPECIFICATIONS FOR RADIO ANECHOIC CHAMBER TESTS

Bandwidth	3.1 to 10.6 GHz
Frequency sweeping samples by VNA	751 samples, 10 MHz interval
IF bandwidth of VNA	100 Hz
SNR at receiver	about 25 dB
Calibration	Internal function of the VNA
Virtual antenna array	$10 \times 2 \times 2$
Element spacing	15 mm
Antennas	UWB omnidirectional antennas

TABLE II.
TEST SCENARIOS FOR RADIO ANECHOIC CHAMBER TESTS

Scenario index		TOA			AOA
		delay τ [ns]	distance [m]	IFFT samples	Azimuth ϕ [°]
A	path 1	3.4	1.02	35	-32
	path 2	6.5	1.96	67	-5
B	path 1	3.4	1.02	35	-32
	path 2	6.1	1.82	62	-29
C	path 1	12.1	3.63	124	-54
	path 2	12.7	3.81	130	55

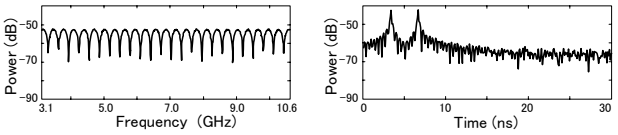

Figure 3. UWB signal model for 2 paths at SNR = 20 dB. (a) FD signal. (b) TD signal.

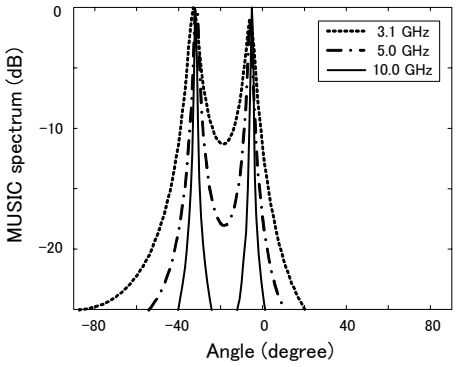

Figure 4. The simulated MUSIC spectra of UWB signal model.

plotted. Note that constant noise power corresponding to the setting SNR was added at each 751 frequency point and the real SNR varied owing to dips, as shown in Fig. 3 (a). However, we selected the initial phase of each FD point to avoid falling in the dips at the four frequencies. The RMSE closes to the CRB rapidly as the frequency increases, as shown in Fig. 5. Although the RMSE for 10.0 GHz coincides with the CRB at SNR $\geq$ 4 dB, the RMSE increases sharply as the SNR decreases. This behavior is referred as the threshold phenomenon [17], [18]. In Fig. 6, we show the impact of TOA subtraction for the RMSE performances. Although the RMSE for 10.0 GHz converges to the CRB at SNR $\geq$ 8 dB, the RMSEs for 3.1, 5.0 and 8.0 GHz stay above the CRB. Since the number of outliers caused by TOA subtraction increases as the frequency decreases, the RMSE of lower frequency after TOA subtraction tend to stay above the CRB even if the SNR goes higher.

We next discuss the RMSE performances of the AOA histogram. The parameters were the same as for Figs. 5 and 6. The AOA histogram is counted for the total 751 of AOA samples, as described in Section 3.B. Then we simulated the AOA histograms before and after the TOA subtraction, as shown in Fig. 7. The RMSE performances before and after the TOA subtraction have very similar behavior and two thresholds occur at SNR = -6, 6 dB. Since the estimated AOA separation is 1° and the number of outliers decreases, two RMSE performances close to the CRB within 3 dB from -6 dB to 6 dB and go to zero at SNR $\geq$ 6 dB. Since rounding off the phase error within 1° leads to the excessive phase error from -6 dB to 6 dB, the accuracy of RMSE with rounding off was worse than that of without rounding off. However, the accuracy of RMSE with rounding off goes to zero at SNR $\geq$ 6 dB owing to rounding off to the correct phase. We see that, for AOA estimation of the UWB both the AOA histogram before and after the TOA subtraction are robust to the RMSE.

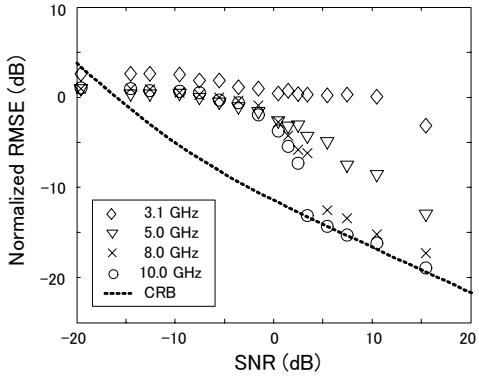

Figure 5. RMSE performances of estimated AOA samples at four frequencies before TOA subtraction.

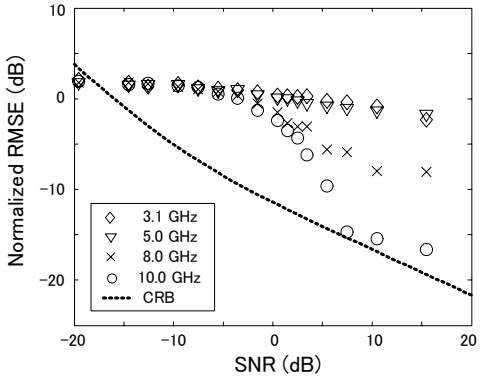

Figure 6. RMSE performances of estimated AOA samples at four frequencies after TOA subtraction.

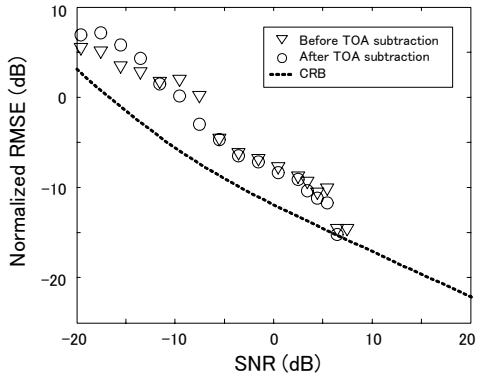

Figure 7. RMSE performances of AOA estimation using AOA histogram before and after TOA subtraction.

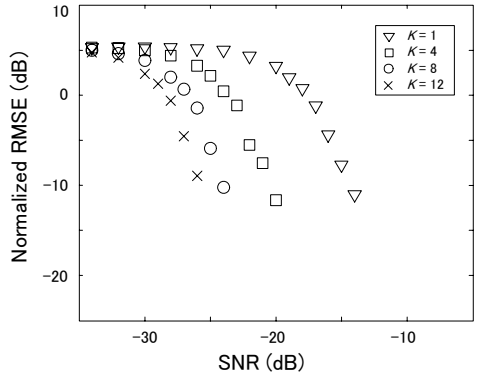

Figure 8. RMSE performances of TOA estimation.

D. RMSE Performances of TOA Estimation

We evaluated the effect of the TD smoothing from the RMSE using the UWB spectrum model except the delay time of the two signals setting 3.4 and 4.4 ns. Since the TD signals are a set of discrete TD samples, the CRB of TOA can not be solved analytically. Therefore we simulated the RMSE of the TOA to evaluate the estimation accuracy, as shown in Fig. 8. The RMSE performances of TOA for four snapshots, K = 1, 4, 8 and 12 at SNR going from -35 dB to -5 dB is plotted.

The RMSEs go to zero where the SNR is higher than the threshold SNR, since the values of delay time errors are within one IFFT sample region. The threshold SNR decreases as the K increases. Since the number of snapshots for the TD smoothing is equivalent to K = 8 and the measured TD signals is equal to K = 1, the TOA estimation using the TD smoothing is more accurate than that of measured TD signals. Increasing the K from 8 to 12 gives much less decrement of threshold SNR than going from 1 to 4, and increasing K yields diminishing returns in terms of the increment of snapshots. This result implies that the TD smoothing averaged over eight temporal samples achieves a certain number of snapshots.

Comparing the threshold SNR of TOA and AOA estimation, we see that the TOA is more robust for the SNR than the AOA, as shown in Figs. 7 and 8. This is the reason why we estimate the TOA before the AOA, as described in Section 3.B.

IV. Tests Conducted in a Radio Anechoic Chamber

A. The Experimental Setup and Measurement

The test system consists of a VNA and a virtual antenna array on the receiver side, as shown in Fig. 2. The measurement was controlled by a computer via GPIB. The transmit and receive antennas were UWB monopole antennas [20] of which group delay was within 0.1 ns. Three test scenarios are listed in Table II. In scenario A and B, two paths were generated using two transmit antennas by a wideband divider with 3 dB power loss. In scenario C, two paths were generated using single transmit antenna and a reflection board. The elevation angle of each path in Table II was within 5° from broadside.

Fig. 9 (a) and (b) show the measured power spectrum and the TD signals for scenario A, respectively. Comparing the ideal signals, as shown in Fig. 3 (a) and (b), the measured power spectrum is not flat and the two peaks on the TD signals are wider than the ideal signal. We consider the differences are caused by the ambiguity of FFT and IFFT conversion owing to the variation of the power level over UWB bandwidth, and several distortion factors of the test system, such as nonlinear parts and antennas.

We implemented the TOA and AOA estimation algorithm, as described in Section 3.B, and then demonstrated the algorithm for three scenarios in Table II.

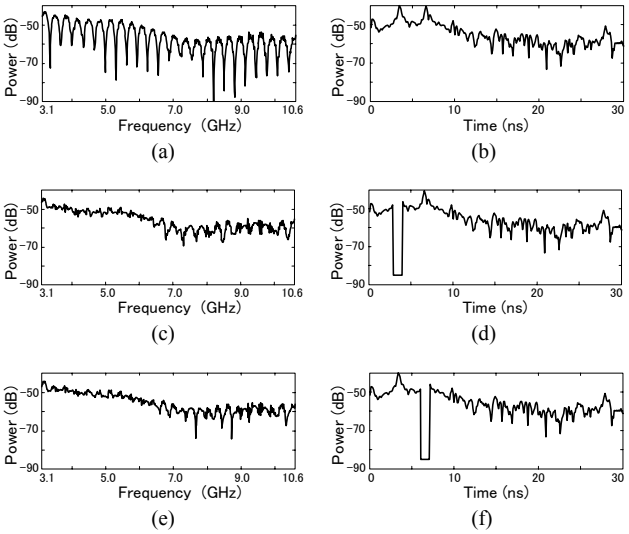

Figure 9. UWB signal spectra for scenario A. (a) Measured spectrum. (b) TD signal taking IFFT with respect to (a). (c) FD signal after TOA τ_1 subtraction. (d) TD signal after TOA τ_1 subtraction. (e) FD signal after TOA τ_2 subtraction. (f) TD signal after TOA τ_2 subtraction.

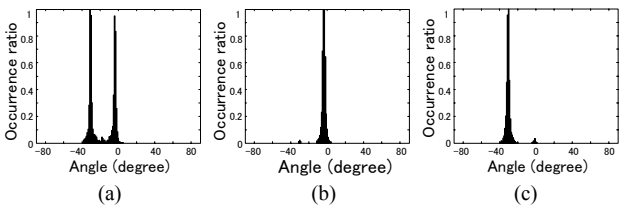

Figure 10. AOA histograms for scenario A. (a) Before TOA subtraction. (b) After TOA τ_1 subtraction. (c) After TOA τ_2 subtraction

B. Test Results of Scenario A

We first consider scenario A, both the TOA and the AOA of each path are resolvable. The results are shown in Figs. 9 and 10. From the algorithm from step 1 to 6, we can obtain the TOA vector $\boldsymbol{\tau} = [\tau_1, \tau_2]^T$ and the AOA vector $\boldsymbol{\phi} = [\phi_1, \phi_2]^T$. In Fig. 9, (a) shows the measured power spectrum consist of 751 samples, there are dips corresponding to the difference of delay times between two paths; (b) shows the TD signals taking IFFT with respect to (a), which can be seen two TOAs, τ_1 of 3.4 ns and τ_2 of 6.5 ns. In Fig. 10 (a), the AOA histogram before TOA subtraction for scenario A is plotted. We can see two AOAs, ϕ_1 of -32° and ϕ_2 of -5°. The number of occurrences is counted for the total 751 of AOA samples every 1°. The occurrence ratio of each angle is obtained by dividing each maximum number of occurrences, since we need to evaluate fairly.

After determining the TOA and AOA vectors, we must pair the element of each vector, processing the algorithm from step 7 to 10. In Fig. 9, (c) shows the FD signals corresponding to (d); (d) shows the TD signals after τ_1 subtraction; (e) shows the FD signals corresponding to (f); (f) shows the TD signals after τ_2 subtraction. The subtraction level -85 dB is set in the range of the x-axis at the center of TOA point plus or minus five points according to the results of the RMSE

evaluation [14]. Comparing the FD signals before and after TOA subtraction, we can see dips of the former were deeper than that of the latter, as shown in Fig. 9 (a), (c) and (e). We also observe that each TOA is subtracted without affecting the other TOA, as shown in Fig. 9 (d) and (f).

The AOA histogram for FD signals after τ_1 subtraction is plotted in Fig. 10 (b). We can determine ϕ_1 as the AOA corresponding to subtracted τ_1, and then two pairs are obtained straightforward, such as τ_1 and ϕ_1, τ_2 and ϕ_2, which correspond to path 1 and 2 of scenario A in Table II. Similarly, we can determine the same two pairs from the AOA histogram for FD signals after τ_2 subtraction, as shown in Fig. 10 (c).

C. Test Results of Scenario B

We next consider scenario B, the TOA of each path is resolvable but two AOAs are too close to resolve. The results are shown in Figs. 11 and 12. Fig. 11 (a) and (b) shows almost the same performances as the results of scenario A in Fig. 9 (a) and (b), respectively. We can see two TOAs, τ_1 of 3.4 ns and τ_2 of 6.1 ns, as shown in Fig. 11 (b). In Fig. 12 (a), the AOA histogram before TOA subtraction for scenario B is plotted. We can observe only single AOA, ϕ_a of -31°. Then we obtain the TOA vector $\boldsymbol{\tau} = [\tau_1, \tau_2]^T$ and the AOA ϕ_a.

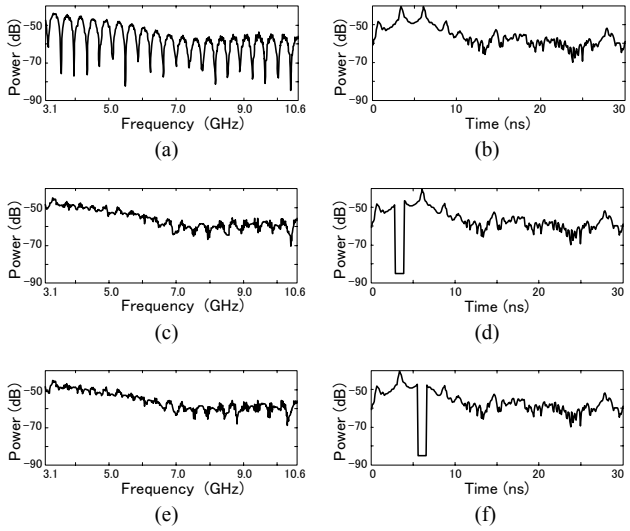

Figure 11. UWB signal spectra for scenario B. (a) Measured spectrum. (b) TD signal taking IFFT with respect to (a). (c) FD signal after TOA τ_1 subtraction. (d) TD signal after TOA τ_1 subtraction. (e) FD signal after TOA τ_2 subtraction. (f) TD signal after TOA τ_2 subtraction.

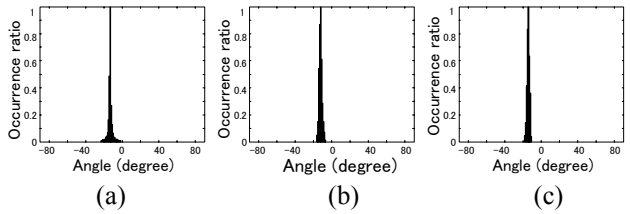

Figure 12. AOA histograms for scenario B. (a) Before TOA subtraction. (b) After TOA τ_1 subtraction. (c) After TOA τ_2 subtraction

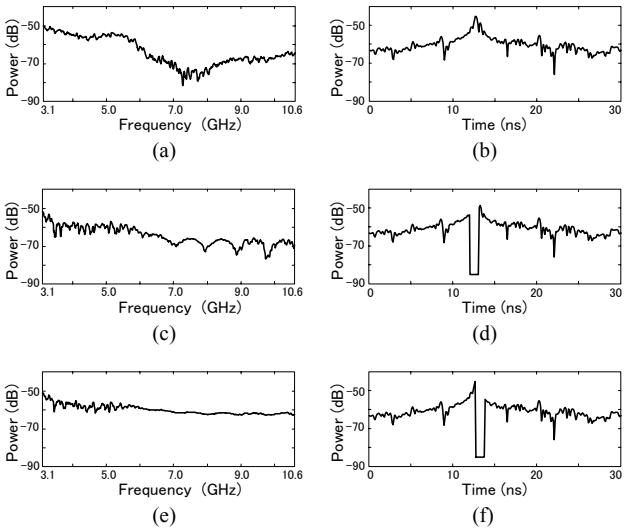

Figure 13. UWB signal spectra for scenario C. (a) Measured spectrum. (b) TD signal taking IFFT with respect to (a). (c) FD signal after TOA τ_1 subtraction. (d) TD signal after TOA τ_1 subtraction. (e) FD signal after TOA τ_2 subtraction. (f) TD signal after TOA τ_2 subtraction.

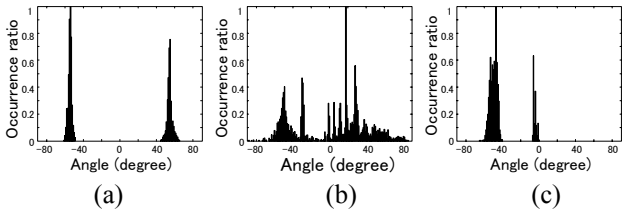

Figure 14. AOA histograms for scenario C. (a) Before TOA subtraction. (b) After TOA τ_1 subtraction. (c) After TOA τ_2 subtraction

We must confirm whether two elements of TOA vector correspond to the AOA, processing the algorithm from step 7 to 10. Fig. 11 (c) to (f) show almost the same performances as the results of scenario A in Fig. 9 (c) to (f), respectively. The AOA histograms after τ_1 and τ_2 subtraction are plotted in Fig. 12 (b) and (c), respectively. The peak corresponding to un-subtracted TOA can be seen, and therefore we can confirm ϕ_a as the AOA corresponding to both subtracted TOAs τ_1 and τ_2. Then we can precisely determine two AOAs ϕ_1 of -32° and ϕ_2 of -29° from peak search in Fig. 12 (c) and (b), respectively. We also obtain two pairs, such as τ_1 and ϕ_1, τ_2 and ϕ_2, which correspond to path 1 and 2 of scenario B in Table II.

D. Test Results of Scenario C

We finally consider scenario C, the AOA of each path is resolvable but two TOAs are too close to resolve. The results are shown in Figs. 13 and 14. In Fig. 13, (a) shows the measured power spectrum, dips are not observed since two paths impinge on the antenna array simultaneously; (b) shows the TD signals taking IFFT with respect to (a), which can be seen only single TOA, τ_a of 12.7 ns. The peak incorporated with two TOAs is wider than the peak of scenario A and B. In Fig. 14 (a), the AOA histogram before TOA subtraction for scenario

C is plotted. We can see two AOAs, ϕ_1 of -54° and ϕ_2 of 55°. Then we obtain the TOA τ_a and the AOA vector $\boldsymbol{\phi} = [\phi_1, \phi_2]^T$.

We must confirm whether two elements of AOA vector correspond to the TOA, processing the algorithm from step 7 to 10. In Fig. 13, (c) shows the FD signals corresponding to (d); (d) shows the TD signals after τ_1 subtraction; (e) shows the FD signals corresponding to (f); (f) shows the TD signals after τ_2 subtraction. Note that τ_1 and τ_2 were split the TOA τ_a into two parts. The AOA histograms after τ_1 and τ_2 subtraction are plotted in Fig. 14 (b) and (c), respectively. We can not easily determine the adequate pairing from Fig. 14 (b) and (c), since the TOA subtraction eliminates the most part of signal components. We therefore confirm τ_a as the TOA corresponding to subtracted both AOAs ϕ_1 and ϕ_2. Moreover, we assume the last half TOA subtraction corresponds to AOAs ϕ_1 of -54°, since the largest peak may correspond to the TOA τ_1 from Fig. 14 (c). Then we can see two TOAs τ_1 of 12.3 ns and τ_2 of 13.0 ns from Fig. 13 (d) and (f), respectively. We also assume two pairs, such as τ_1 and ϕ_1, τ_2 and ϕ_2. The assumptions are adequate because of closely corresponding to path 1 and 2 of scenario C in Table II.

V. Conclusion

This paper has presented a technique for the UWB channel estimation using transformation between TD and FD signals. We propose the TOA and AOA estimation algorithm for two paths, as described in section 3.B. Then we simulate the RMSE of estimated TOA and AOA, and demonstrate in anechoic chamber tests. The proposed algorithm is able to resolve the TOAs and the AOAs precisely, even if either TOAs or AOAs are too close to resolve. There are four main advantages of the proposed estimation scheme as follows: implementation of the simple antenna array with fixed element spacing; the TOA and estimation using a peak search over TD signals with high resolution; the AOA estimation using the 1-D MUSIC and AOA histograms over FD signals; pairing the elements of TOAs and that of AOAs precisely using each TOA subtraction for TD signals.

These advantages for two paths can be applied to more complex propagation environments. We have been developing three paths estimation scheme [15] and indoor channel estimation scheme [16] based on the proposed TOA and AOA estimation scheme.

Acknowledgment

This work has been supported in part by a grant from the Ministry of Internal Affairs and Communications of Japan within its Strategic Information and Communications R & D Promotion Programme, and in part by the Research Institute for Science and Technology, Tokyo Denki University, under the grant Q06J-02.

References

[1] B. H. Fleury, M. Tschudin, R. Heddergott, D. Dahlhaus, and K. I. Pedersen, "Channel parameter estimation in mobile radio environments using the SAGE algorithm," *IEEE J. Sel. Areas Commun*., vol. 17, no. 3, pp. 434-449, Mar. 1999.

[2] K. Kalliola, H. Laitinen, L. I. Vaskelainen, and P. Vainikainen, "Real-time 3D spatial–temporal dual-polarized measurement of wideband radio channel at mobile station," *IEEE Trans. Instrum. Meas*., vol. 49, no. 2, pp. 439–448, Apr. 2000.

[3] K. Sakaguchi, J. Takada, and K. Araki, "A novel architecture for MIMO spatio–temporal channel sounder," *IEICE Trans. Electron*., vol. E85-C, no. 3, pp. 436–441, Mar. 2002.

[4] R. E. Bethel and K. L. Bell, "Maximum likelihood approach to joint array detection/estimation," *IEEE Trans. Aerosp. Electron. Syst*., vol. 40, no. 3, pp. 1060-1072, Jul. 2004.

[5] K. Haneda, J. Takada, and T. Kobayashi, "A parametric UWB propagation channel estimation and its performance validation in an anechoic chamber," *IEEE Trans. Microwave Theory and Techniques*, vol. 54, no. 4, pp. 1802-1811, Apr. 2006.

[6] R. J-M. Cramer, R. A. Scholtz, and M. Z. Win, "Evaluation of an ultra-wide-band propagation channel," *IEEE Trans. Antennas Propag*., vol. 50, no. 5, pp. 561-570, May 2002.

[7] W. Ciccognani, A. Durantini, and D. Cassioli, "Time domain propagation measurements of the UWB PN-sequence in the FCC-compliant band 3.6-6 GHz," *IEEE Trans. Antennas Propag*., vol. 53, no. 4, pp. 1542-1549, Apr. 2005.

[8] J. Zhang, R. A. Kennedy, and T. D. Abhayapala, "Cramér-Rao Lower Bounds for the time delay estimation of UWB signals," in *Proc. IEEE Int. Conf. Commun*., Jun. 2004, pp. 3424-3428.

[9] C. Carbonelli and U. Mitra, "Clustered channel estimation for UWB signals," in *Proc. IEEE Int. Conf. Commun*., Jun. 2004, pp. 2432-2436.

[10] R. J. Cramer, R. A. Scholtz, and M. Z. Win, "Evaluation of an ultrawide-band propagation channel," *IEEE Trans. Antennas Propag*., vol.50, no. 5, pp. 561–570, May 2002.

[11] M. Z. Win and R. A. Scholtz, "Characterization of ultra-wide bandwidth wireless indoor channels: A communication-theoretic view," *IEEE J. Select. Areas Commun*., vol. 20, no. 9, pp. 1613–1627, Dec. 2002.

[12] P. J. Chung and J. F. Böhme, "Comparative convergence analysis of EM and SAGE algorithms in DOA estimation," *IEEE Trans. Signal Process*., vol. 49, no. 12, pp. 2940-2949, Dec. 2001.

[13] P. J. Chung and J. F. Böhme, "Recursive EM and SAGE-inspired algorithms with application to DOA estimation," *IEEE Trans. Signal Process*., vol. 53, no. 8, pp. 2664-2677, Aug. 2005.

[14] N. Iwakiri and T. Kobayashi, "Joint TOA and AOA estimation of UWB signal using time domain smoothing", in *Porc. 2nd International Symposium on Wireless Pervasive Computing 2007*, San Juan, Puerto Rico, No. 23, Feb. 2007.

[15] N. Iwakiri and T. Kobayashi, "Ultra-wideband channel estimation using a signal model based on measurements", *IEICE Trans. Fundamentals Electron. Commun. Comput. Sci.*, Nov. 2007, to be published.

[16] N. Iwakiri and T. Kobayashi, "Ultra-Wideband Indoor Channel Estimation Using a Signal Model Based on

Measurements", in *Porc. 2nd European Conference on Antennas and Propagation*, Edinburgh, UK, Nov. 2007, to be published.
[17] H. L. V. Trees, *Optimum Array Processing*. New York: Wiley, 2002.
[18] C. D. Richmond, "Capon algorithm mean-squared error threshold SNR prediction and probability of resolution," *IEEE Trans. Signal Process*., vol. 53, no. 8, pp. 2748-2764, Aug. 2005.
[19] H. Krim and M. Viberg, "Two decades of array signal processing research," *IEEE Signal Process. Mag*., vol. 13, pp. 67–94, Jul. 1996.
[20] T. Taniguchi, A. Maeda, and T. Kobayashi, "Development of an omni-directional and low-VSWR ultra wideband antenna," *Int. J. on Wireless & Optical Commun*., vol. 3, no. 2, pp. 145–157, 2006.

Naohiko Iwakiri received his B.E. degree in electrical Engineering from Dosishya University, Kyoto, Japan. His professional career includes Japan Radio Co., Ltd., Tokyo, Japan; Sony Corporation, Tokyo, Japan; where he was engaged in research and development of digital signal processing and various wireless communication systems, such as CDMA cellular, wireless LAN and UWB systems. From 1995 to 1999, he was with YRP Key Tech. Labs, Yokosuka, Japan, which focused on the 4 th generation mobile communication systems. Currently, he is pursuing a Ph. D. degree at the Tokyo Denki University.

His research interests are in general areas in wireless communication systems, statistical and adaptive signal processing for digital communications, and communication theory and information theory. His current research focuses on wideband wireless channel estimation and signal processing in MIMO systems, and associated computational analysis and system design.

Takehiko Kobayashi received the B.E., M.E., and Ph.D. degrees in electrical engineering from the University of Tokyo, Tokyo, Japan, in 1978, 1980, and 1983. In 1983, he joined Nippon Telegraph and Telephone, where he was engaged in research on various wireless communication systems. In 1986, he was a guest scientist with the National Bureau of Standards (now the National Insitute of Standards and Technology), Boulder, CO. From 1998 to 2001, he was with YRP Key Tech Labs, where he focused on fourth-generation mobile communication systems. He is currently a Professor with the Department of Information and Communication Engineering, Tokyo Denki University, Tokyo, Japan. He received the IEICE Best Paper Awards in 2001 and 2002 and the Telecom System Awards from the Telecommunications Advancement Foundation in 2003 and 2005. His current research interests include UWB wireless systems, mobile communication channel characterization, and teletraffic evaluation of mobile communication networks.